ORIGINAL RESEARCH

Optimization of Photon Counting CT Myelography for the Detection of CSF-venous Fistulas Using Convolutional Neural Network Denoising: A Comparative Analysis of Reconstruction Techniques

Ajay A. Madhavan, MD, Zhongxing Zhou, MD, Paul J. Farnsworth, MD, Jamison Thorne, Timothy J. Amrhein, MD, Peter G. Kranz, MD, Waleed Brinjikji, MD, Jeremy K. Cutsforth-Gregory, MD, Michelle L. Kodet APRN, CNP, MSN, Nikkole M. Weber RT, Grace Thompson, Felix E. Diehn, MD, Lifeng Yu, MD[1]

ABSTRACT

BACKGROUND AND PURPOSE: Photon counting detector CT myelography is a recently described technique used for detecting spinal CSF leaks, including CSF-venous fistulas. Various image reconstruction techniques, including smoother versus sharper kernels and virtual monoenergetic images, are available with photon counting CT. Moreover, denoising algorithms have shown promise in improving sharp kernel images. No prior studies have compared image quality of these different reconstructions on photon counting CT myelography. Here, we sought to compare several image reconstructions using various parameters important for the detection of CSF-venous fistulas.

MATERIALS AND METHODS: We performed a retrospective review of all consecutive decubitus photon counting CT myelograms performed between 2/1/2022 and 8/1/2024 at one institution. We included patients whose studies had the following reconstructions: Br48-40 keV virtual monoenergetic reconstruction, Br56 low energy threshold (T3D), Qr89-T3D denoised with quantum iterative reconstruction, and Qr89-T3D denoised with a convolutional neural network algorithm. We excluded patients who had extradural CSF on preprocedural imaging or a technically unsatisfactory myelogram. All four reconstructions were independently reviewed by two neuroradiologists. Each reviewer rated spatial resolution, noise, presence of artifacts, image quality, and diagnostic confidence (whether positive or negative) on a 1-5 scale. These metrics were compared using the Friedman test. Additionally, noise and contrast were quantitatively assessed by a third reviewer and compared.

RESULTS: The Qr89 reconstructions demonstrated higher spatial resolution than their Br56 or Br48-40keV counterparts. Qr89 with convolutional neural network denoising had less noise, better image quality, and improved diagnostic confidence compared to Qr89 with quantum iterative reconstruction denoising. The Br48-40keV reconstruction had the highest contrast-to-noise ratio quantitatively.

CONCLUSIONS: In our study, the sharpest quantitative kernel (Qr89-T3D) with convolutional neural network denoising demonstrated the best performance with regards to spatial resolution, noise level, image quality, and diagnostic confidence for detecting or excluding the presence of a CSF-venous fistula.

ABBREVIATIONS: CNR = contrast-to-noise ratio; CVF = CSF-venous fistula; EID = energy integrating detector; PCD = photon counting detector; PCD-CTM = photon counting detector CT myelography; ROI = region of interest; SNR = signal-to-noise ratio; SIH = spontaneous intracranial hypotension; T3D = low-energy threshold; UHR = ultra-high resolution.

Received month day, year; accepted after revision month day, year.
From the Department of Radiology (A.A.M, Z.Z, P.J.F, J.T., W.B, J.K.C-G, M.L.K, N.M.W, G.T, F.E.D., L.Y.), Mayo Clinic, Rochester, MN, USA and the Department of Radiology (T.J.A, P.G.K), Durham, NC, USA.

The authors declare no conflicts of interest related to the content of this article.

Please address correspondence to Ajay A. Madhavan, MD, Department of Radiology, Mayo Clinic, 200 1st St. SW, Rochester, MN, 55905, USA; madhavan.ajay@mayo.edu

SUMMARY SECTION

PREVIOUS LITERATURE: Recent studies have described the use of decubitus photon counting CT myelography for the detection of CSF-venous fistulas, one of the most common causes of spontaneous intracranial hypotension. Relatively few specific techniques for photon counting CT myelography have been described, and no prior studies have specifically assessed different kernel reconstructions or denoising algorithms in a comparative fashion.

KEY FINDINGS: We found that the sharpest quantitative kernel used in photon counting CT myelography (Qr89) with convolutional neural network denoising provided the best image quality and diagnostic confidence with respect to detecting CSF-venous fistulas.

KNOWLEDGE ADVANCEMENT: This is the first study assessing different kernels and denoising algorithms on photon counting CT myelography. Our findings may be helpful to institutions implementing this technique in their practices.

INTRODUCTION

Photon counting detector CT (PCD CT) is a relatively new but increasingly used technology for a variety of applications in neuroradiology. PCD CT myelography (PCD-CTM) was recently described for the detection of spinal CSF leaks in patients with spontaneous intracranial hypotension (SIH).[1-4] This includes both prone and decubitus PCD-CTM, which are used for the precise localization of dural tears and CSF-venous fistulas (CVFs), the two most common causes of SIH.[4, 5] CVFs can be particularly elusive on imaging, sometimes necessitating multiple myelograms using different imaging modalities for confident detection.[6, 7] PCD-CTM holds great promise in this regard, having shown a relatively high diagnostic yield for CVF detection in recent studies.[8] Although PCD CT has many advantages over traditional energy integrating detector (EID) CT, its most important advancement for CVF detection is improved spatial resolution.[9] The intrinsic multi-energy acquisition and spectral imaging capability while scanning at a fast speed are additional benefits of PCD-CTM that may aid in CVF detection.[10]

Many different image reconstruction options are available on PCD CT, including a wide spectrum of smooth to sharp kernels.[11] Smoother kernels generally have a higher contrast-to-noise ratio (CNR) but lower spatial resolution for any given section thickness. Sharper kernels have higher spatial resolution but greater image noise, resulting in a lower CNR. Since electronic noise is reduced in PCD CT through low-energy thresholding, sharper kernels have better image quality compared to their EID CT counterparts. Sharp kernel images can be further denoised in post-processing to improve image quality, with previously described techniques including quantum iterative reconstruction (QIR, Siemens Healthineers) and a deep learning-based dedicated high resolution convolutional neural network (CNN).[12-14] A prior case series highlighted the value of CNN denoising for improving the conspicuity of CVFs.[14] PCD CT also has the option to perform virtual monoenergetic imaging (VMI) because of the detector's inherent spectral sensitivity, obviating the need to use specific dual energy or dual source imaging modes.

To date, no studies have evaluated the different imaging reconstructions available for PCD-CTM. Here, we sought to compare four different reconstruction techniques currently used in our PCD-CTM protocol. Namely, these include Br48 40 keV VMI (Br48-40keV), Br56 low energy threshold / T3D (Br56), Qr89 T3D denoised using QIR at a strength of 4 (Qr89 QIR-4), and Qr89 T3D denoised with a dedicated high resolution CNN (Qr89-CNN). These Br and Qr reconstructions were initially included in our routine PCD-CTM protocol because they provide high resolution and result in relatively little distortion of normal anatomy compared to other options. Based on our anecdotal experience, we hypothesized that Qr89-CNN would be the most preferred and most useful reconstruction for detecting or excluding CVFs.

MATERIALS AND METHODS

Patient Selection

This study was deemed exempt by our institutional IRB. A standard STROBE checklist was used to assist in study design. We performed a retrospective review of all consecutive decubitus photon counting CT myelograms performed between 2/1/2022 and 8/1/2024 at our institution. Note that all patients met International Classification of Headache Disorder criteria (third edition) for SIH, based on our institutional workflow for performing these exams (brain MRI abnormalities or low CSF opening pressure). We excluded any patients whose myelograms did not include all the following reconstructions: Br48-40keV, Br56, Qr89 QIR-4, and Qr89-CNN.[14] We also excluded patients who had extradural CSF on preprocedural spine imaging, since this would indicate the presence of a dural tear rather than a CVF. Finally, we excluded any technically unsatisfactory studies that would potentially be nondiagnostic (substantial motion artifact or inadvertent subdural/intradural injections) on the basis of preliminary image review by a single neuroradiologist.

Image Acquisition

Our precise technique for PCD-CTM has been previously described.[8] Right and left decubitus scans were obtained using the ultra-high resolution (UHR) mode (Naeotom Alpha, Siemens Healthineers), and all reconstructions were generated from these scans. Section thickness was 0.2 mm for Br56, 0.2 mm for Qr89 QIR-4, 0.2 mm for Qr89-CNN, and 0.4 mm for Br48-40keV (0.4 mm is the lowest slice thickness allowable for 40 keV reconstructions). For dynamic (multiphase) studies, only the final UHR scan was used for the analysis. This was done to ensure that all included images were obtained after injection of the full intrathecal bolus of contrast (typically 5-8 mL of Omnipaque 300, GE Healthcare). Furthermore, only either the right or left decubitus portion of the exam was used: if a CVF was detected on the exam based on the imaging report, the side harboring the CVF was chosen for the analysis. If a CVF was not detected, a random side was chosen.

Image Review

For included patients, Br48-40keV, Br56. Qr89 QIR-4, and Qr89-CNN series were uploaded into a new research PACS session. All four reconstructions were independently reviewed in a blinded fashion by two neuroradiologists, both of whom routinely perform and interpret PCD-CTM exams and have 3 and 8 years of post-fellowship experience. The reconstructions were presented in a random order in our PACS, and all imaging identifiers and imaging reports were removed. Note that the non-denoised Qr89 images (reconstructed with filtered back projection) were not included in the analysis, since they are typically non-diagnostic (Figure 1).

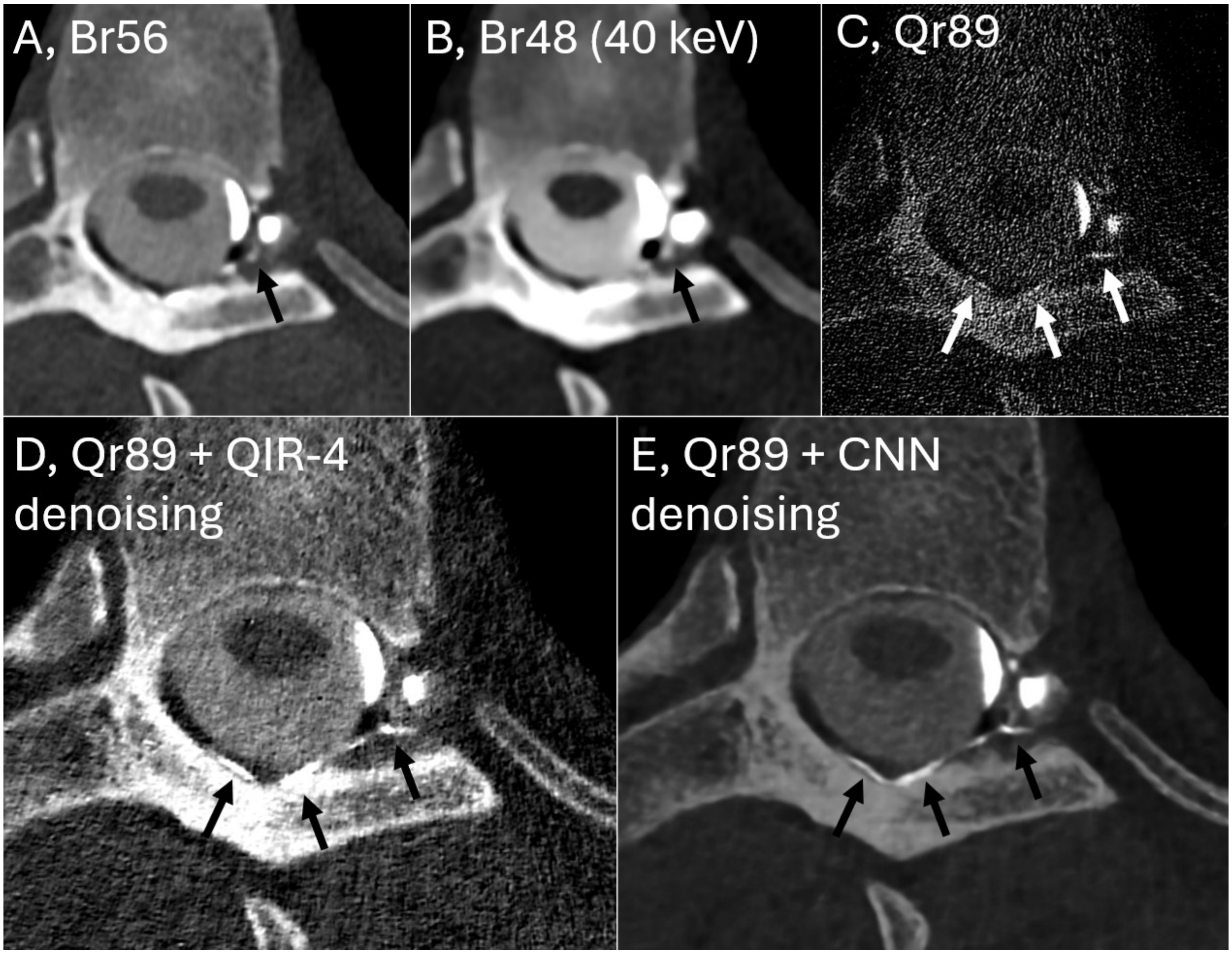

FIG 1. Example of different imaging reconstructions analyzed in this study, highlighting the value of sharp kernels with denoising. Images from a left decubitus photon counting CT myelogram, all from the same slice and with the same window/level setting, demonstrate a left T7 CSF-venous fistula draining into the dorsal internal epidural venous plexus (A-E, arrows). The fistula is poorly visualized on the Br56 (A) and Br48 40 keV (B) reconstructions, as there is insufficient spatial resolution to discriminate the vein from the adjacent lamina. The Qr89 image (C) has better spatial resolution, but the diagnostic quality is markedly degraded by noise on this sharper kernel. Denoising the Qr89 images with either QIR-4 (D) or CNN (E) technique substantially improves image quality, with the fistula best seen on the Qr89 + CNN denoised image (E, arrows).

Each reviewer initially evaluated all available reconstructions and assessed whether one or more CVFs was present. This portion of the assessment was dichotomous (positive or negative). Next, reviewers subjectively rated spatial resolution, noise level, presence of artifacts, image quality, and diagnostic confidence (whether positive or negative for CVF) on a 1-5 scale (Likert score), with a rating of 5 always indicating superiority (higher resolution, less noise, fewer artifacts, better perceived image quality, and higher diagnostic confidence).

Next, noise and contrast were quantitatively assessed by a third reviewer. Noise was measured by placing a region of interest (ROI) over the paraspinal musculature at the level of T12 and recording standard deviation of CT attenuation number. A 5 mm diameter ROI was used for all noise measurements. Contrast was measured as the mean CT attenuation number of the intrathecal contrast bolus at T12 (measured with a 1 mm ROI) minus the mean CT attenuation number measured over the paraspinal musculature at T12. This method is in keeping with a recent study assessing noise and contrast on PCD CT angiography.[15]

Statistical analysis

Mean and standard deviations of Likert scores were calculated for individual readers and averaged scores between both readers. The Friedman test was used to compare averaged Likert scores for each condition, with a P value < 0.05 indicating a statistically significant difference. For the quantitative analysis, mean and standard deviation contrast and noise values were calculated across all four reconstructions. CNR was calculated by dividing the contrast by the noise and compared across the four conditions, with a p value less than 0.05 indicating a statistically significant difference (Friedman).

RESULTS

Patient cohort

We initially identified 140 unique patients who underwent one single-day, bilateral decubitus PCD-CTM. A total of 101 patients were excluded from the study: 80 patients were excluded, because their PCD-CTM did not include all of the desired imaging reconstructions (Br48-40keV, Br5, Qr89 QIR-4, and Qr89-CNN); 21 patients were excluded since their preprocedural imaging showed extradural CSF, compatible with an underlying dural tear rather than CVF. No patients were excluded on the basis of technically unsuccessful studies. In total, 39 adult patients remained in the study (mean age 52.5±15.9 years). 20/39 (51.3%) patients were women.

A single CVF was identified in 20/39 (51.3%) of patients, with the remaining 19/39 (49.7%) of patients' studies being negative. There was complete agreement between both readers in this regard, and the readers' findings were concordant with imaging reports in all cases.

Reader Evaluation Analysis (Figure 2)

Spatial Resolution

Mean Qr89-CNN and Qr89 QIR-4 scores were superior to other conditions (Qr89-CNN: 5; Qr89 QIR-4: 4.9±0.15; Br56: 3.2±0.5; Br48-40keV: 3.1±0.3; $p < 0.001$).

Image Quality

Qr89-CNN was superior in comparison to the other conditions (Qr89-CNN: 4.9±0.3; Br56: 3.9±0.4; Qr89 QIR-4: 3.4±0.5; Br48-40keV: 3.4±0.4; $p < 0.001$).

Diagnostic Confidence

Qr89-CNN was superior compared to the other conditions (Qr89-CNN: 4.9±0.3; Br56: 3.9±0.4; Qr89 QIR-4: 3.7±0.5; Br48-40keV: 3.6±0.6; $p < 0.001$).

Artifacts

Image artifacts rated in similar fashion across all conditions (Qr89-CNN: 4.2±0.5; Br56: 3.9±0.3; Br48-40keV: 3.7±0.7; Qr89 QIR-4: 3.8±0.5; $p > 0.999$).

Noise

Noise rated highest (indicating less noise) for Qr89-CNN closely followed by Br56. Both Qr89-CNN and Br56 were superior compared to the other conditions (Qr89-CNN: 4.4±0.6; Br56: 3.9±0.3; Br48-40keV: 3.4±0.5; Qr89 QIR-4: 2.1±0.4; $p < 0.001$).

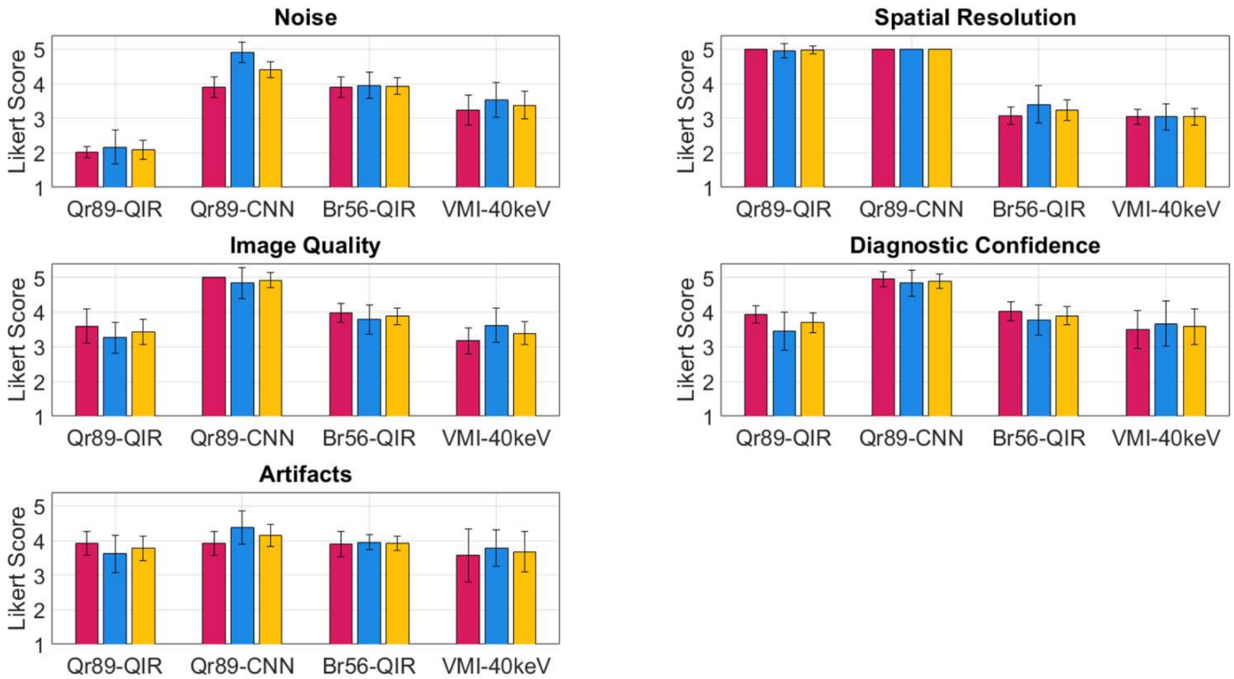

FIG 2. Bar plots illustrating the mean Likert scores for each reconstruction evaluated in this study (red = reader 1, blue = reader 2, yellow = average of both readers). For each category, a higher score indicates a stronger preference for the given reconstruction. Thin vertical lines represent the standard deviation.

Quantitative Analysis (Supplemental Figure 1)

Br48-40keV had significantly higher average contrast measurements compared to the rest of the modalities (Br48-40keV: 10627.6±2834.2; Br56: 3595.7±973.7; Qr89 QIR-4: 3393±881.4; Qr89-CNN: 3362±879.1; $p < 0.001$). Noise measurements were significantly higher for Qr89 QIR-4 compared to the rest of the modalities (Qr89 QIR-4: 119.9±30; Br48-40keV: 42.7±6.3; Qr89-CNN: 38.1±4.2;Br56: 33.2±7.4; $p < 0.001$). CNR proved most favorable on the Br48-40keV images, while least favorable on Qr89 QIR-4 images (Br48-40keV: 255.2±84.5; Br56: 112.3±40.7; Qr89-CNN: 89±27.6; Qr89 QIR-4: 29.7±10.5; $p<0.001$).

DISCUSSION

In this study, we sought to compare four different PCD-CTM image reconstructions on the basis of spatial resolution, noise, presence of undesirable artifacts, image quality, and diagnostic confidence for detecting or excluding a CVF.

We found that Qr89-CNN, the sharpest quantitative kernel denoised with a deep learning-based algorithm, provided the highest diagnostic confidence and greatest perceived image quality on the basis of ratings from two expert reviewers. This appeared to be due to the combination of very high spatial resolution and low noise level provided by this reconstruction. The Qr89 images with QIR-4 denoising showed similarly high spatial resolution; however, these images had greater noise. Presumably as a result of this, the Qr89 QIR-4 images were rated similar to the Br56 and Br48-40 keV VMIs and lesser than Qr89-CNN images with respect to diagnostic confidence and image quality. Our findings are in keeping with recent studies demonstrating the clinical superiority of Qr89-CNN images for various PCD CT applications.[15, 16]

Based on our quantitative analysis of contrast and noise on the four different reconstructions, the Br48-40 keV VMIs had the highest CNR. This was presumably due to the higher iodinated contrast attenuation conferred at this low monoenergetic level. Despite having a higher quantitative CNR, however, the 40 keV VMIs were rated as equal or lesser to Qr89-CNN in every subjective category. This result would suggest that quantitative CNR measurements do not necessarily predict reader preferences. Also of interest, Qr89-CNN had a lower quantitative noise level and higher CNR than Qr89 QIR-4. This observation is in keeping with our qualitative analysis of the images, in which Qr89-CNN was generally preferred over Qr89 QIR-4.

The findings of this study are clinically important. Since the initial description of CVFs in 2014, imaging techniques to detect these often-subtle lesions have improved substantially.[17] Decubitus digital subtraction myelography (DSM), EID CTM, cone beam CTM (CB-CTM), and PCD-CTM have emerged as valuable techniques for CVF detection, each having particular advantages and disadvantages.[18, 19] Optimization of post-processing techniques remains a relatively unexplored method of improving CVF conspicuity. Our findings underscore the importance of refining this aspect of CTM. In particular, we believe that efforts to improve spatial resolution while maintaining CNR are paramount. High spatial resolution is frequently necessary to confidently identify CVFs and discern them from normal anatomic structures (Figure 3 and Supplemental Figure 2). Even in cases where CVFs are detected using modalities with lower resolution, high resolution modalities such as PCD-CTM may offer superior characterization of the fistula and aid in treatment planning (Figure 4).

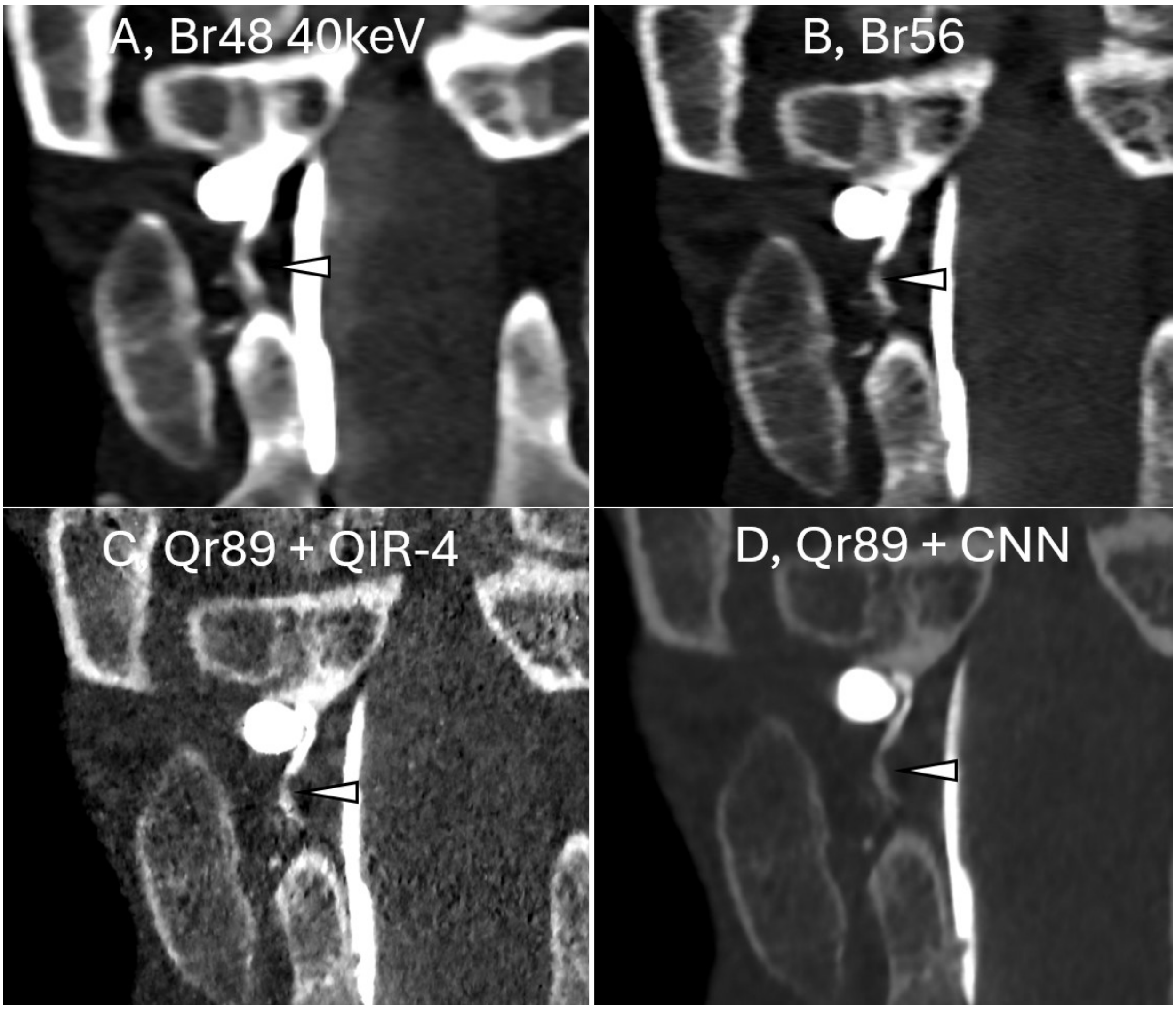

FIG 3. Advantage of Qr89-CNN images to detect of a right T7 CSF-venous fistula involving the internal epidural venous plexus (A-D, arrowheads). The portion of the fistula medial to the diverticulum is poorly visualized on the coronal Br48 40keV (A) and Br56 (B) reconstructions (A-B, arrowheads), because the spatial resolution is not sufficient to differentiate the vein from the diverticulum. The fistula is better characterized on the Qr89 QIR-4 image (C, arrowhead) and best seen on the Qr89-CNN image (D, arrowhead).

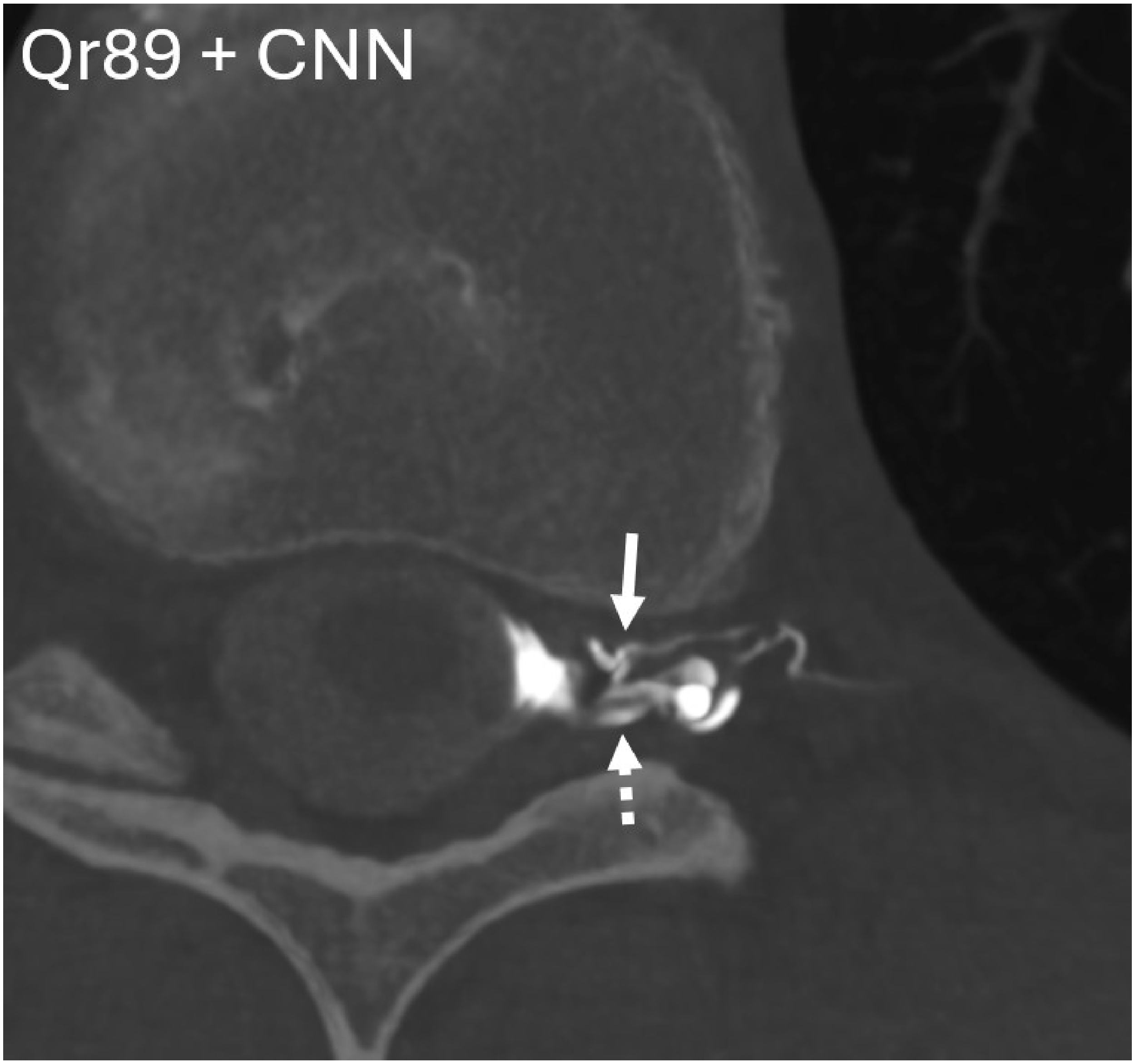

FIG 4. Axial Qr89 CNN denoised image from a photon counting CT myelogram, demonstrating precise anatomic characterization of a left T10 CSF-venous fistula. The origin of the fistula from the neck of a left T10 diverticulum is well-characterized (solid arrow). Normal anatomy, such as the nerve root within its dural sleeve, is also exquisitely seen (dashed arrow).

Our study has limitations. First, our sample size was relatively small. Since not all studies in our database had the desired reconstructions available, some patients had to be excluded. Second, our comparison of different reconstructions was limited to those routinely used in our practice, even though PCD CT has many other kernels and available options for image reconstruction. Upon starting PCD-CTM in our practice, we selected these four based on internal review of several choices, which was partially informed by our prior clinical experience. Finally, our methodology for assessing different reconstructions was partially subjective. Future studies assessing multiple kernels, different VMI energy levels, and other post-processing options, perhaps in a multi-institutional fashion, would be beneficial to validate our findings. This would also help to potentially reproduce our findings with more patients. Additionally, since our CNN denoising algorithm is currently only available at our institution, similar studies on other CNN algorithms would be helpful.

CONCLUSIONS

Our study comparing four different post-processing options for PCD-CTM showed that the Qr89-CNN denoised reconstruction was superior to Qr89 with QIR-4 denoising, Br56, and Br48-40keV VMIs with respect to diagnostic confidence for CVF detection. This was largely a result of two key factors: 1) the Qr89 kernel provided the highest spatial resolution and 2) CNN denoising more effectively reduced noise on this sharp kernel compared to QIR-4.

REFERENCES

1. Madhavan AA, Yu L, Brinjikji W, et al. Utility of Photon-Counting Detector CT Myelography for the Detection of CSF-Venous Fistulas. *AJNR Am J Neuroradiol* 2023;44:740-744
2. Schwartz FR, Malinzak MD, Amrhein TJ. Photon-Counting Computed Tomography Scan of a Cerebrospinal Fluid Venous Fistula. *JAMA Neurol* 2022;79:628-629
3. Schwartz FR, Kranz PG, Malinzak MD, et al. Myelography Using Energy-Integrating Detector CT Versus Photon-Counting Detector CT for Detection of CSF-Venous Fistulas in Patients With Spontaneous Intracranial Hypotension. *AJR Am J Roentgenol* 2024
4. Madhavan AA, Cutsforth-Gregory JK, Brinjikji W, et al. Benefits of Photon-Counting CT Myelography for Localization of Dural Tears in Spontaneous Intracranial Hypotension. *AJNR Am J Neuroradiol* 2024
5. Mamlouk MD, Ochi RP, Jun P, et al. Decubitus CT Myelography for CSF-Venous Fistulas: A Procedural Approach. *AJNR Am J Neuroradiol* 2021;42:32-36
6. Madhavan AA, Brinjikji W, Cutsforth-Gregory JK, et al. Myelographic Techniques for the Localization of CSF-Venous Fistulas: Updates in 2024. *AJNR Am J Neuroradiol* 2024;45:1403-1412
7. Callen AL, Timpone VM, Schwertner A, et al. Algorithmic Multimodality Approach to Diagnosis and Treatment of Spinal CSF Leak and Venous Fistula in Patients With Spontaneous Intracranial Hypotension. *AJR Am J Roentgenol* 2022;219:292-301
8. Madhavan AA, Cutsforth-Gregory JK, Brinjikji W, et al. Diagnostic Performance of Decubitus Photon-Counting Detector CT Myelography for the Detection of CSF-Venous Fistulas. *AJNR Am J Neuroradiol* 2023;44:1445-1450
9. Mamlouk MD, Callen AL, Madhavan AA, et al. Spinal CSF Leaks: The Neuroradiologist Transforming Care. *AJNR Am J Neuroradiol* 2024
10. Rajendran K, Petersilka M, Henning A, et al. First Clinical Photon-counting Detector CT System: Technical Evaluation. *Radiology* 2022;303:130-138
11. Marth AA, Marcus RP, Feuerriegel GC, et al. Photon-Counting Detector CT Versus Energy-Integrating Detector CT of the Lumbar Spine: Comparison of Radiation Dose and Image Quality. *AJR Am J Roentgenol* 2023:1-9
12. Sartoretti T, Landsmann A, Nakhostin D, et al. Quantum Iterative Reconstruction for Abdominal Photoncounting Detector CT Improves Image Quality. *Radiology* 2022;304:E55
13. Huber NR, Ferrero A, Rajendran K, et al. Dedicated convolutional neural network for noise reduction in ultra-high-resolution photon-counting detector computed tomography. *Phys Med Biol* 2022;67
14. Madhavan AA, Cutsforth-Gregory JK, Brinjikji W, et al. Application of a Denoising High-Resolution Deep Convolutional Neural Network to Improve Conspicuity of CSF-Venous Fistulas on Photon-Counting CT Myelography. *AJNR Am J Neuroradiol* 2023;45:96-99
15. Diehn FE, Zhou Z, Thorne JE, et al. High-Resolution Head CTA: A Prospective Patient Study Comparing Image Quality of Photon-Counting Detector CT and Energy-Integrating Detector CT. *AJNR Am J Neuroradiol* 2024;45:1441-1449
16. Baffour FI, Huber NR, Ferrero A, et al. Photon-counting Detector CT with Deep Learning Noise Reduction to Detect Multiple Myeloma. *Radiology* 2023;306:229-236
17. Schievink WI, Moser FG, Maya MM. CSF-venous fistula in spontaneous intracranial hypotension. *Neurology* 2014;83:472-473
18. Madhavan AA, Lutzen N, Cutsforth-Gregory JK, et al. Additional Diagnostic Value of Cone Beam CT Myelography Performed After Digital Subtraction Myelography for Detecting CSF-venous Fistulas. *AJNR Am J Neuroradiol* 2024
19. Madhavan AA, Brinjikji W, Cutsforth-Gregory JK, et al. Myelographic Techniques for the Localization of CSF-Venous Fistulas: Updates in 2024. *AJNR Am J Neuroradiol* 2024

SUPPLEMENTAL FILES

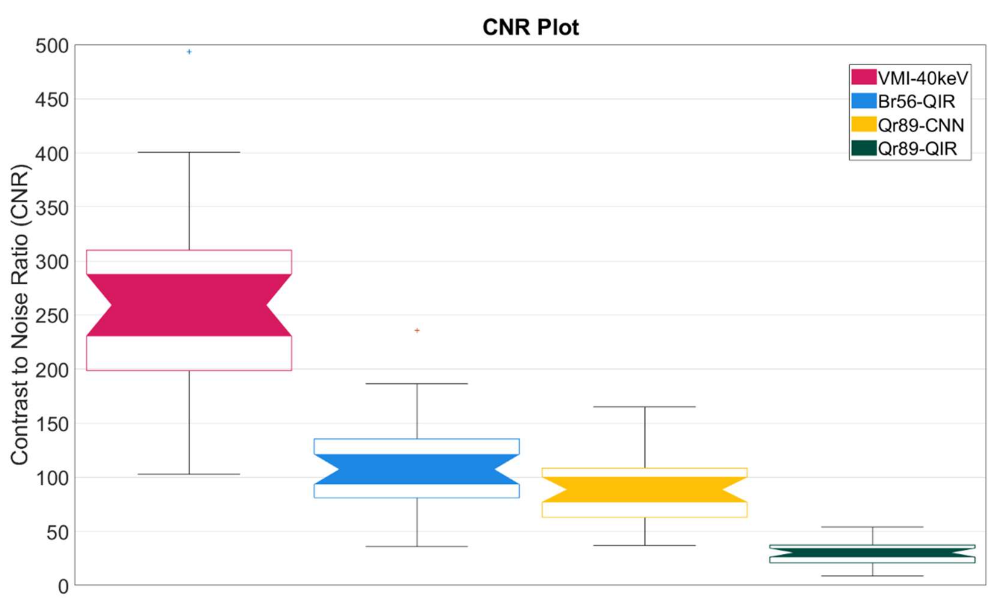

Supplementary Fig 1. Grouped boxplots representing the contrast-to-noise ratio for the four different reconstructions in the study. Center boxes represent the interquartile range, while the center lines correspond to the upper and lower quartiles. Samples whose notches do not overlap are significantly different at the 95% confidence level.

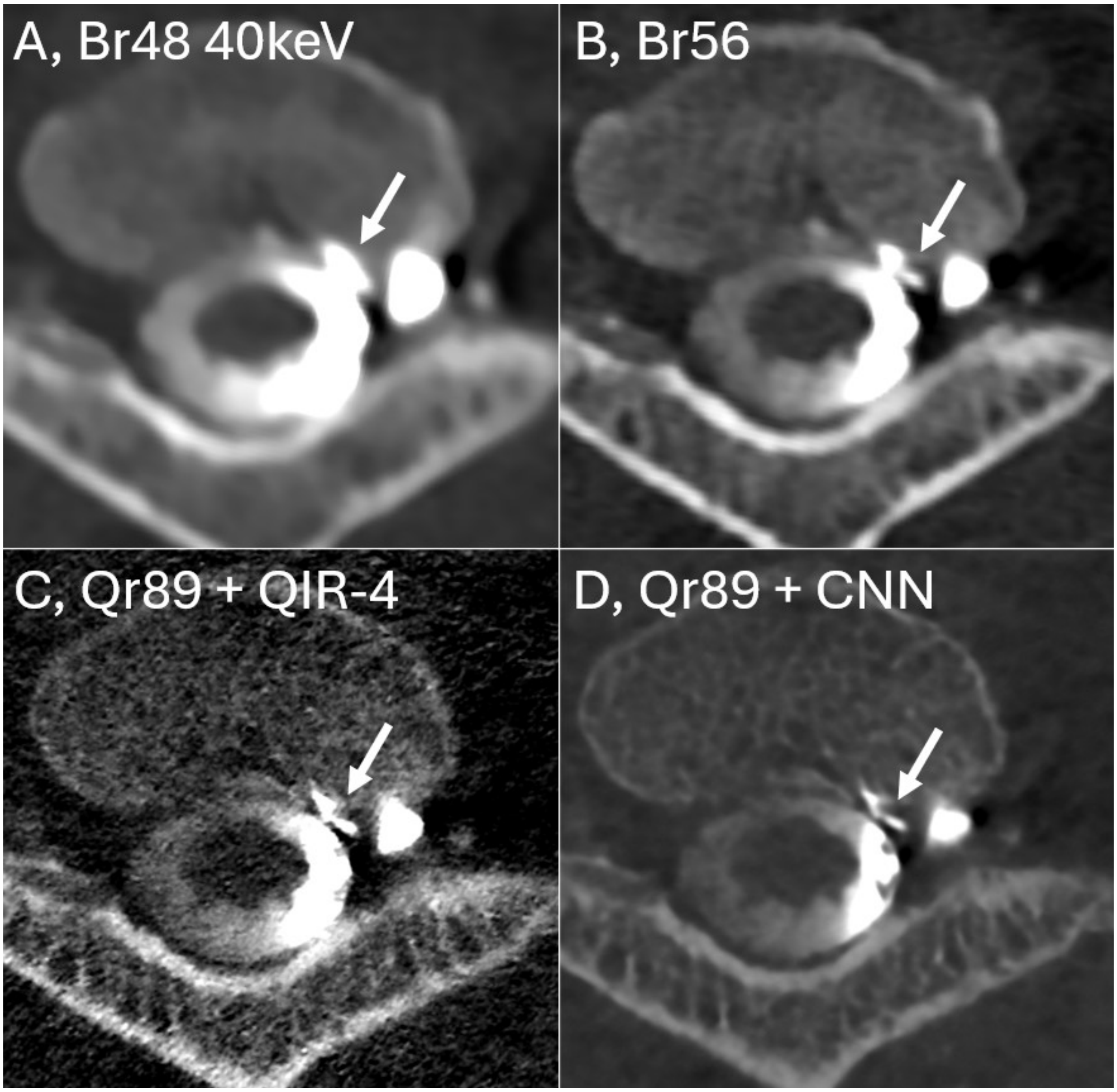

Supplemental Fig 2. Use of a sharper kernel with denoising to differentiate a CSF-venous fistula from a bilobed meningeal diverticulum. Br48 40 keV (A), Br56, Qr89 QIR-4, and Qr89 CNN images at the same slice and window/level setting show a left T1 CSF-venous fistula involving the ventral internal epidural venous plexus and vertebral intraosseous veins (A-D, arrows). Before employing the sharper Qr89 kernel, the finding was thought to potentially represent a medial projecting lobe of a meningeal diverticulum (A-B, arrow), but the linear morphology appreciated on the Qr89 images confirmed that this was in fact a CSF-venous fistula (C-D, arrows).